LUND UNIVERSITY

INITIAL INSIGHTS INTO THE STRUCTURE-ACTIVITY RELATIONSHIPS OF AVIAN DEFENSINS.

Derache, Chrystelle; Meudal, Herve; Aucagne, Vincent; Mark, Kevin J; Cadene, Martine; Delmas, Agnes F; Lalmanach, Anne-Christine; Landon, Celine

Link to publication

INITIAL INSIGHTS INTO THE STRUCTURE-ACTIVITY RELATIONSHIPS OF AVIAN DEFENSINS

Chrystelle Derache[1,2, #], Hervé Meudal[1], Vincent Aucagne[1], Kevin J. Mark[1, $], Martine Cadène[1], Agnès F. Delmas[1], Anne-Christine Lalmanach[2*], Céline Landon[1*]

[1] Centre de Biophysique Moléculaire. CNRS UPR4301. Rue Charles Sadron, 45071 Orléans, France.
[2] Unité Infectiologie Animale et Sante Publique, INRA UR1282, Centre de Recherche de Tours, 37380 Nouzilly, France.
[#] Present address: Medical Microbiology, Department of Laboratory Medicine Malmö, Lund University, Skåne University Hospital, Malmö, Sweden.
[$] Present address: Chemistry Department, York College, Jamaica, NY 111451, USA.

Running title: Structural determinants for the AvBD2 antibacterial activity

[*]To whom correspondence should be addressed: Céline Landon, Centre de biophysique moléculaire, CNRS UPR4301. Rue Charles Sadron, 45071 Orléans, France, phone number +332 38 25 55 74, fax number : +332 38 63 15 17, Email address : celine.landon@cnrs-orleans.fr; Anne-Christine Lalmanach, INRA, UR1282, IASP 213, Centre de recherche de Tours, 37380 Nouzilly, France, phone number : +332 47 42 77 00, fax number : +332 47 42 77 74, Email address : Anne-Christine.Lalmanach@tours.inra.fr

Background: Avian defensins are antimicrobial peptides of bird's immunity.
Results: The target of chicken AvBD2 defensin is not chiral. Its structure is not amphipathic. The reduced and AvBD2-K31A forms dramatically decrease antibacterial activity.
Conclusion: AvBD2 may disrupt the bacterial membrane through a non-chiral non-specific interaction.
Significance: Knowledge of the structure-function relationships of avian defensins is a prerequisite for their use as alternatives to antibiotics.

SUMMARY

Numerous β-defensins have been identified in birds and the potential use of these peptides as alternatives to antibiotics has been proposed, in particular to fight antibiotic-resistant and zoonotic bacterial species. Little is known about the mechanism of antibacterial activity of avian β-defensins (AvBDs), and the present work was carried out to obtain initial insights into the involvement of structural features or specific residues in the antimicrobial activity of chicken AvBD2. Chicken AvBD2 and its enantiomeric counterpart were chemically synthesized. Peptide elongation and oxidative folding were both optimized. The similar antimicrobial activity measured for both L- and D- proteins clearly indicates that there is no chiral partner. Therefore the bacterial membrane is in all likelihood the primary target. Moreover, this work evidences that the three-dimensional fold is required for an optimal antimicrobial activity, in particular for Gram-positive bacterial strains. The three-dimensional NMR structure of chicken AvBD2 defensin displays the structural 3-stranded antiparallel β-sheet characteristic of β-defensins. The surface of the molecule does not display any amphipathic character. In light of this new structure and of the king penguin AvBD103b defensin structure, the consensus sequence of avian β-defensin's family was analyzed. Well conserved residues were highlighted and the potential strategic role of the lysine 31 residue of AvBD2 emphasized. The synthetic AvBD2-K31A variant displayed substantial N-terminal structural modifications and a dramatic decrease in activity. Taken together, these results demonstrate the structural as well as the functional role of the critical lysine 31 residue in antimicrobial activity.

Defensins belong to a family of antimicrobial peptides characterized by cationicity, small size, β-sheet structure and the presence of three disulfide bonds (1). Three subclasses (α, β, and θ) have been defined depending on the disulfide arrangement and the positioning of the six conserved cysteines. The α- and θ-defensin families have been considered to evolve by duplication and divergence from β-defensin ancestor genes since the former are not reported in evolutionary old vertebrates such as fish and bird classes. Defensins play a major role in both innate and adaptive immunity (2). They have been found to be constitutively or inducibly expressed by neutrophils and epithelial cells from many mammals and birds, including chicken (1,3,4). They display a wide range of microbicidal or microbistatic activities against Gram-negative and Gram-positive bacteria, fungi and viruses (4). A substantial body of evidence indicates that the mechanism of action of defensins mainly relies on several structural features such as cationicity and amphipathy, which drive the antimicrobial peptide to interact with bacterial membranes and tend to divide peptides into two mechanistic classes: membrane disruptive and non-membrane disruptive (5,6). In the latter case, there is growing evidence that defensins induce killing by acting on chiral anionic intracellular targets (see (7,8) for a review).

Interest in defensins as therapeutic drugs is growing because defensins may constitute an alternative to the controversial use of antibiotics. In birds, a potential use of these peptides has been proposed in particular to fight antibiotic-resistant bacteria including *Salmonella,* a major zoonotic agent that causes food poisoning (9). Numerous β-defensins were identified in birds from isolated peptides or gene sequences (see (4) for a review). In a previous study, it was shown that chicken β-defensin genes (*avBD1* and *2*) were highly expressed in the intestinal tissue of birds that are resistant to *Salmonella* colonisation (10). Three defensins (AvBD1, AvBD2 and AvBD7) were therefore purified from chicken bone marrow and their antimicrobial activity was tested on a series of Gram-positive and Gram-negative bacteria (11). Only chicken AvBD2 was shown to be more active against Gram-positive than Gram-negative strains, as reported for the king penguin spheniscin (AvBD103b) (12), the only other avian β-defensin whose three-dimensional structure has been determined to date.

Concerning the molecular patterns involved in the activity of avian defensins, the sole data currently available refer to ostrich AvBD1 and AvBD2 defensins, which respectively share 39 and 78% of identity with chicken AvBD2. Ostrich defensins were shown to create a slow and partial depolarization of the *Escherichia coli* membrane, but were unable to provoke bacterium death by membrane disruption (13). This indicated that the ostrich defensins could cross the bacterial membrane to target a cytoplasmic molecule. Considering that the ostrich defensins were efficient in shifting the mobility of bacterial DNA in a gel electrophoresis assay, it has been proposed that DNA could be the defensin's target (13). In the context of the long-term objective of improving knowledge of immunity in birds, this work was carried out to gain information on structure-activity relationships of the chicken AvBD2 defensin, at the atomic level, which is an essential first step to understanding how avian β-defensins function.

EXPERIMENTAL PROCEDURES
Reversed Phase High Performance Liquid Chromatography - HPLC analyses were carried out on either an Elite LaChrom system composed of a Hitachi L-2130 pump, a Hitachi L-2455 diode array detector and a Hitachi L-2200 autosampler, or a LaChrom 7000 system composed of a Merck-Hitachi L-7100 pump, a Merck-Hitachi L-7455 diode array detector and a Merck-Hitachi D-7000 interface, which was also used for semi-preparative purification. The machines were equipped with C18 reversed phase columns, Nucleosil, 300 Å, 5 μm, 250 ×4.6 mm for the analytical separations, or 250 ×10.5 mm for purification. Solvents A and B containing 0.1% of TFA (trifluoroacetic acid) were H_2O and MeCN, respectively.
Synthesis of the linear, S-alkylated defensins – Solid-phase peptide synthesis (SPPS) was run on an automated synthesizer 433A from Applied Biosystem using Fmoc/*t*-Bu chemistry at a 0.1 mmol scale with HBTU (*O*-(benzotriazol-1-yl)-*N*,*N*,*N′*,*N′*-tetramethyluronium hexafluorophos-phate) / HOBt (1-hydroxybenzotriazole hydrate) as the coupling reagent. Fmoc-Ala-methylphenoxypropionic acid (Polypeptide group, France) (122 mg, 0.25 mmol) was manually coupled onto the aminomethyl PEGA (polyethylene glycol polyacrylamide) resin (3 g wet, 0.1 mmol) in the presence of HATU (*O*-(7-aza-benzotriazol-1-yl)-*N*,*N*,*N′*,*N′*-tetramethyl-

uronium hexafluorophosphate) (95 mg, 0.25 mmol) and DIEA (*N,N*-diisopropylethylamine) (86 μl, 0.5 mmol) for 2 h. The elongation was then carried out automatically using a 10-fold excess of protected amino acids and coupling reagents. The protecting groups used for the side-chains were Arg(Pbf), Asn(Trt), Cys(Acm), His(Trt), Lys(Boc), Ser(*t*-Bu), Trp(Boc), Tyr(*t*-Bu). A 0.1 mmol scale program was used, and each coupling step was followed by capping with acetic anhydride. The coupling step was performed twice from Cys30 to Leu1. The dipeptides Gly7-Ser8 and Gly31-Ser32 were also coupled twice, as the Fmoc-Gly-Ser($\Psi^{Me,Me}$ pro)-OH pseudoproline derivative (Merck). After completion of the peptide elongation, the peptide resin was treated for 3 h at room temperature with TFA/H_2O/*i*-Pr_3SiH/PhOH, 87.5:5:2.5:5, and the linear *S*-Acm-alkylated peptide was precipitated by dilution into ice-cold diethyl ether.

Synthesis of the oxidized defensins - In a syringe fitted with a frit, the *S*-Acm-protected peptide resin (15 μmol) was swollen in NMP (2 x 5 mL for 1 min). Silver tetrafluoroborate (58.4 mg per Acm group, 20 equiv.) in NMP/H_2O 9:1 mixture (4 ml) was transferred to the resin by suction, and the resulting suspension was stirred by rotation for 5 min at RT, in the absence of light, followed by washes with NMP/H_2O 9:1 then DMF. This treatment was repeated once (60 min stirring), and the resin was further washed with pyridine (5 x 6 ml), then treated alternatively with sodium diethyldithiocarbamate (25 mM in NMP) and pyridine hydrochloride (1M in CH_2Cl_2/MeOH 95:5) (3 x 2 x 5 ml), followed by extensive washes with DMF. The peptide resin was then treated for 3 h at room temperature with TFA/H_2O/*i*-Pr_3SiH/PhOH, 87.5:5:2.5:5 and the linear peptide was precipitated by dilution with ice-cold diethyl ether. The crude reduced form of AvBD2 was dissolved in 20% acetic acid (AcOH) and purified by semi-preparative C18 reversed phase HPLC.

The oxidative folding was performed at a peptide/GSH/GSSG molar ratio of 1/100/10 in deoxygenated MeCN/200 mM Tris-HCl buffer pH 8.5 (50/50, v/v) containing 1 mM EDTA. The peptide concentration (50 μg/mL) was measured using UV spectrophotometry at 280 nm (ε_{Trp}: 5579 M^{-1} cm^{-1}). The kinetics of the oxidative folding were monitored by quenching, at regular time intervals, aliquots from the reaction mixture through the addition of TFA (final concentration 2%), and then analyzing the

sample by analytic C18 reversed phase HPLC. The oxidative folding was quantitative over 30 min. The peptide was purified on to a Resource S column (GE Healthcare Biosciences) using a linear gradient of 0–0.5M NaCl in 50 mM Tris pH7.5. The fractions corresponding to the pure peptide were loaded on a Sep-Pak® C18 (6ml column, Waters) followed by washings with 5% aqueous AcOH, and eluted by MeCN/H_2O/AcOH 5:4:1 and lyophilized.

Mapping of disulfide bridges by proteolytic cleavage and mass spectrometry

Proteolytic cleavage - Protein cleavages were performed in a total volume of 20 μL. To avoid the scrambling of disulfide bridges known to occur at basic pH, cleavages were performed in 30 mM ammonium acetate buffer adjusted to pH 6.5. Trypsin (Roche Diagnostics) cleavage of AvBD2 was performed at an enzyme:substrate ratio of 1:20 (w/w) for 4 hours at 37°C. Papain (Roche Diagnostics) was incubated with AvBD2 for 4 hours at 25°C using an enzyme:substrate ratio of 1:5 (w/w). For papain cleavage, the following amino acids were considered for proteinase specificity: Arg, Ala, Asn, Asp, Glu, Gln, Gly, His, Lys, Phe, Leu, and Tyr.

Mass spectrometry - Intact and proteolyzed synthetic ʟ-AvBD2 were analyzed by Matrix Assisted Laser Desorption Ionization-Time of Flight (MALDI-TOF) using an Autoflex instrument (BrukerDaltonics, Bremen, Germany) equipped with a 337-nm nitrogen laser and a gridless delayed extraction ion source. Sample deposition on the MALDI plate was performed using the ultrathin layer method as previously described (14,15). Samples were diluted at a ratio of 1:20 with a matrix solution consisting of 4-hydroxy α-cyanocinnamic acid (4HCCA, Bruker) saturated in a solution of 66.5% water, 33.3% MeCN and 0.1% TFA. A 0.5 μL aliquot of this analyte-matrix solution was spotted onto the ultrathin layer plate. The MALDI spot was irradiated using a 4 Hz laser pulse to produce ions. At least 200 laser shots were accumulated for each spectrum. Ions were analyzed in positive ion reflector mode with a 150 ns delay and an accelerating voltage of 19 kV. The measured *m/z* values correspond to the a0 peak as determined by the SNAP algorithm on the isotopic ion distribution. The spectra were calibrated externally and internally using the Pepmix calibrant mixture (Bruker) consisting of bradykinin, angiotensin, substance P, bombesin, renin substrate, adrenocorticotropic hormone 19-38 and somatostatin. Instrument parameters were

adjusted using FlexControl (Bruker). Data analysis and internal calibration were performed using FlexAnalysis (Bruker). The disulfide-bridged cleavage peptides were mapped to the known AvBD2 sequence using the PeptideMap software tool from the PROWL website at http://prowl.rockefeller.edu (The Rockefeller University, New York, USA). Given the amino acid sequence of the protein and the proteinase cleavage specificity, PeptideMap automatically computes all theoretically possible combinations of bridged peptides and matches the observed masses to the corresponding theoretical masses.

Antimicrobial activity test - The antibacterial activities of the peptides were measured by radial diffusion assay (16) as described in Derache *et al. (11)* in gel containing either one of the following Gram-positive bacterial strains: *Bacillus cereus* ATCC 14579, *Staphylococcus aureus* ATCC 29740, and *Listeria monocytogenes* strain EGD, or one of the following Gram-negative bacterial strains: *Escherichia coli* ATCC 25922, *Salmonella enterica* serovar Enteritidis ATCC 13076, and *Salmonella enterica* serovar Typhimurium ATCC 14028. For each bacterial strain, three identical independent measurements of the antibacterial activity were performed. The minimal inhibitory concentration (MIC) of each peptide was determined from a graph constructed by plotting the log peptide concentration against the diameter of the clear zone on the plate minus the diameter of the well. The best-fit straight-line was determined using linear regression with GraphPad Prism 5 software (GraphPad Software). The MIC was calculated by finding the x-intercept of the line, indicating the peptide concentration at which no clear zone is obtained. For each bacterial strain, the statistical difference between native and variant peptide MICs was assessed by comparing the slope and intercepts of both regression lines with GraphPad Prism 5 software (GraphPad Software). The level of significance was set at $P < 0.05$.

Circular Dicroism experiments - The CD experiments were carried out on a Jasco J-810 spectropolarimeter. Solutions of 30μM (10mM Phosphate buffer pH 7.2) of both L-AvBD2 and D-AvBD2 enantiomers were compared.

Three-dimensional NMR structure - A standard set of 2D ^{1}H-NMR experiments (COSY, 80ms TOCSY, and 160ms NOESY) was performed, on a 0.1 mM aqueous solution of the synthetic L-AvBD2 (H_2O/D_2O 90/10 and 100% D_2O) at pH 4.1, and at 293K. An additional set of data,

recorded at 303K, was used to resolve assignment ambiguities due to spin system overlaps. All spectra were recorded on a BRUKER 800 MHz spectrometer (NMR facilities, Gif-sur-Yvette, France). The NMR data sets were processed using the NMRPipe/NMRDraw software package (17,18). ^{1}H chemical shifts were assigned according to classical procedures (19). NOE cross-peaks were integrated and assigned within the NMRView software (17). Covalent bonds were built between the sulfur atoms of the paired cysteines. Structure calculations were performed with the ARIA 1.1 software (20). The calculations were initiated using the default parameters of ARIA and a first set of easily assigned NOEs. At the end of each run, the new assignments proposed by ARIA were checked manually and introduced (or not) in the following calculation. This iterative process was repeated until complete assignment of the NOESY map. A last run of 1000 structures was then performed with the final list of NOE derived distance restraints, and 200 structures were submitted to the last step on ARIA. The 10 structures without residual NOE violation and with the lowest residual NOE energy were selected and considered as characteristic of the peptide structures. Representation and quantitative analysis of the calculated structures were performed using MOLMOL (21) and in-house programs.

The same sets of experiments were recorded on a VARIAN 600MHz spectrometer for the variant AvBD2-K31A (2.4 mM of the synthetic peptide in aqueous solution at pH 4.2, and at 293K). The same protocol was followed except that ambiguous constraints were introduced between cysteine residues, using the "ambiguous disulfide bridges" protocol of the ARIA 1.1 software (20).

RESULTS

Chemical synthesis of AvBD2: chemical and functional characterization *versus* extracted AvBD2.

The peptide elongation of AvBD2 was carried out by solid phase peptide synthesis (SPPS) following the Fmoc/*t*-Bu strategy. Besides repeating most of the coupling steps twice, optimisation of the elongation yield required the combined use of pseudoproline dipeptide derivatives and a polar resin (22). Our synthetic strategy also involved the use of the acetamidomethyl (Acm) group as a TFA-stable protection of cysteinyl residues to obtain the linear *S*-Acm-alkylated AvBD2 (AvBD2-Acm).

To obtain the linear non-alkylated AvBD2 from the same batch of peptide resin, we developed conditions for the removal of the Acm groups on the peptide resin before the final TFA treatment. After HPLC-purification of the reduced form of AvBD2, the oxidative folding was carried out using a procedure based on a thermodynamically controlled disulfide shuffling, in the presence of reduced and oxidized glutathione at pH 8.5. The folding kinetics was followed by quantitative analytical HPLC and the reaction was shown to be complete in 30 min (Fig. S1 in supplementary data). MALDI-TOF MS analysis of oxidized AvBD2 showed a 6 Da difference in mass compared to the reduced form, consistent with the fully oxidized form of this peptide (data not shown). The oxidized AvBD2 was then purified to homogeneity by cation exchange chromatography. Reversed phase HPLC analysis showed that synthetic AvBD2 co-eluted with the natural product extracted from chicken bone marrow (Fig. S2 in supplementary data). As further evidence of the identity of the synthetic and natural peptides, their activities measured in minimal inhibitory concentration (MIC) assays were in the same range for every bacterial strain tested (supplementary material Table S3). Altogether, our data validated an efficient optimized protocol for the production of highly pure and biologically active synthetic AvBD2. It was successfully applied to the synthesis of the all-D enantiomeric homologue of AvBD2 (D-AvBD2) and the AvBD2-K31A variant (Fig. S4). The all-D form was checked by circular dichroïsm where CD spectra of the two enatiomers show equal and opposite spectra (Fig. S5). In the case of the AvBD2-K31A variant, the increase in hydrophobicity led to a poor folding yield. Organic solvents were then screened as folding additives (Table S6 in supplementary data) and MeCN, which greatly enhanced the yields, was selected for preparative scale oxidative foldings. Our optimized protocol including an efficient peptide elongation and the use of a co-solvent for the folding step enabled an enhanced production yield up to 30-40% for all the AvBD2 peptides.

Antibacterial activity

The antimicrobial activities of D-AvBD2 and L-AvBD2 were tested on a selection of three Gram-positive (*B. cereus, L. monocytogenes* and *S. aureus*) and three Gram-negative (*E. coli, S. Enteritidis* and *S.* Typhimurium) bacterial strains. As shown on Table 1, the MICs

measured for the two enantiomers are identical for every tested strain.

To investigate the role of the well-conserved three-dimensional frame of β-defensin in AvBD2 functionality, the antibacterial activities of the linear *S*-alkylated AvBD2 (AvBD2-Acm) were compared with the activities of its oxidatively folded counterpart (Table 1). The linear AvBD2-Acm is less active than the folded AvBD2 for every bacterial strain tested except for *E. coli* (P=0.06), as shown by the dramatic increase in the MIC of AvBD2 when linear. In particular, the linear form of AvBD2 is 10 and 16 times less efficient than the folded peptide against the Gram-positive strains *B. cereus* (P=0.0002) and *L. monocytogenes* (P=0.0002), respectively. The linear form is even ineffective in our conditions towards the Gram-positive strain *S. aureus*, showing the strict requirement of the three-dimensional fold for an optimal antimicrobial activity. The effect of the three-dimensional structure on the activity is more limited for the Gram-negative strains. Indeed, for *S.* Enteritidis and *S.* Typhimurium, the linear form of AvBD2 displays an activity one and a half (P<0.0001) to three times (P=0.0002) lower than that of the folded AvBD2 peptide.

AvBD2 solution structure

Partial determination of AvBD2 disulfide bridges array

The determination of the correct disulfide pairing is generally achieved using enzymatic proteolysis of proteins and mass spectrometry analysis of the obtained cleavage products. These data can thus be introduced as additional constraints in structure calculations, allowing the three-dimensional models to converge more efficiently. For the chicken AvBD2 defensin, the trypsin proteolysis experiment produced cleavage peptides which were identified by MALDI-TOF MS. The observed masses were matched to four sets of disulfide-connected peptides using the PeptideMap software (Table S7 in supplementary data). While peptides Leu1-Lys4 and Val20-Arg27 each contain one connectable cysteine, peptides Gly5-Lys19 and Ser28-Lys31 each have two cysteines which can participate in disulfide bridges. The connection of Leu1-Lys4 to Ser28-Lys31 shows that Cys3 is connected to Cys29 or Cys30. Similarly, Cys23 has to be linked to either Cys8 or Cys13. These first two connected products were observed with one linked cysteine and one free thiol. The products containing three connected peptides show that the remaining cysteine, either

8 or 13, forms a bond with the remaining cysteine 29 or 30. Trypsin cleavage thus narrowed down the number of possible disulfide bridges combinations to four (Fig. S8 in supplementary data). Papain proteolysis produced one set of connected peptides, defining the Cys8-Cys23 bridge for certain. Consequently, in keeping with the trypsin result showing that Cys13 does not connect with Cys3, Cys13 can only connect with Cys29 or Cys30. However, these adjacent cysteines could not be differentiated. It is a known limitation of this method that, because of the impossibility to cleave between adjacent half-cystinyl residues, connected peptides containing a single disulfide bond cannot be obtained in such cases (22). Following analyses by enzymatic proteolysis combined with mass spectrometry, software computation and logical deduction, among the fifteen possibilities for the disulfide bridges array, only two remained: 3-29, 8-23, 13- 30 or 3-30, 8-23, 13-29. On NMR NOESY maps, one connectivity was observed between one of the β-protons of Cys8 and the β-protons of Cys23, confirming the Cys8-Cys23 pairing determined from mass spectrometry data. The chemical shifts of β-protons of Cys3, Cys13, Cys29 and Cys30 were very close, therefore NOE peak superimpositions and/or proximity of diagonal peaks hampered unambiguous assignments. The sole unambiguous observed connectivity was between the β-protons of Cys13 and one of the β-protons of Cys30, even if very close to the diagonal, arguing for the 13-30 disulfide bridge.

AvBD2 three-dimensional NMR structure
The quality of the NMR spectra acquired with the 280 µg of synthetic L-AvBD2 (see sequence Fig.1) allowed the assignment of all proton resonances. Chemical shifts have been deposited in the BioMagResBank (http://www.bmrb.wisc.edu/) with the entry code 17797. NOE peaks were picked and integrated in NMRView. A first set of about 200 intra-residues, sequential and easily-determined long-range peaks were assigned. Additional assignments were progressively proposed during the ARIA runs (20), and manually validated. The use of ambiguous intersulphur distances, an option assuming that a given half-cystine is part of a bridge without supposing a particular partner, could not be successfully applied for AvBD2. This method is considered as a reliable and robust method for disulfide-rich proteins (23), but the calculations did not converge satisfactorily enough, even based on a very

convenient set of NOEs (around 15 NOEs – including 3 long-range restraints each). Therefore it was more convenient to add the disulfide bridges as constraints. The two remaining possibilities were compared: 3-29, 8-23, 13-30 or 3-30, 8-23, 13-29. Convergence to a well-formed 3-stranded beta-sheet was only obtained in the first case, with a convenient residual number of NOE violations, and satisfactory energies. The last iterations to refine the structure were then performed with the 3-29, 8-23, 13-30 disulfide bridges array. The final numbers of distance restraints used in the last run of ARIA calculations are detailed in Table 2. The solution structures of AvBD2 were represented by ten conformers refined in a shell of water (Fig. 2 A), and were deposited in the Protein Data Bank (http://www.pdb.org) with the 2gl5 entry code. The three-dimensional structure of AvBD2 displays the structural characteristics of β-defensins: a three-stranded antiparallel β-sheet, (7-9; 18-22; 28-31) stabilized by a conserved array of three disulfide bridges. The sequential Cys29 and Cys30 belong to the middle strand of the β-sheet, therefore their side chains point in opposite directions. The measured distances greater than 8 Å between the sulfur atoms of Cys13 and Cys29, or between Cys3 and Cys30, definitively preclude the possibility of C1-C6; C2-C4; C3-C5 pairing that could match NOE NMR data. The structures were in very good agreement with the experimental data; there was no violation of distance restraints larger than 0.3 Å. Most of the residues (92.7%) were found in the most favorable regions of the Ramachandran plot. On the whole, the secondary structure elements were well defined, and the RMSD value calculated for secondary structures was 0.62 Å (table 2). The analysis of the surface properties clearly evidenced that the positive and hydrophobic residues were well distributed on the three-dimensional structure of the molecules (Fig. 2B and 2C). Contrary to many antibacterial molecules, AvBD2 did not display any amphipathic character, neither along the primary structure (Fig. 1) nor on the three-dimensional structure of the molecules (Fig. 2).

Three-dimensional NMR structure and antibacterial activity of AvBD2-K31 variant
The protocol applied for AvBD2 was followed for AVBD2-K31A except that ambiguous constraints were introduced between cysteine residues, using the "ambiguous disulfide bridges" option. In the first calculations each half-cystine was allowed to be linked to one of

the 5 others, leading to 15 possibilities of pairing. During the calculations, each disulphide bridge is then allowed to float freely and the protocol is driven to the most compatible disulfide bridges array, under the influence of the other NMR restraints. Once aberrant conformations (bridging more than 2 sulfur atoms) were discarded, a majority (72%) of structures correspond to the "3-29, 8-23, 13-30" disulfide bridges array, the residual 28% corresponding to the "3-30, 8-23, 13-29" pairing. At this stage, comparing two parrallel calculations differing only by the disulfide bridges array imposed: 3-29, 8-23, 13-30 or 3-30, 8-23, 13-29, only the first calculations converged to a well-formed 3-stranded beta-sheet. In the second calculations, the strands could not form properly. There was 25% more NOE violations, and the total energy was multiplied by 2. The refinement of the structure in the last iterations was then performed with the 3-29, 8-23, 13-30 disulfide bridges array.

A very accurate model of AvBD2-K31A variant was determined by NMR (the RMSD value calculated for secondary structures is 0.19 Å; Table 2). The structures were in very good agreement with the experimental data, and most of the residues (96.2%) were found in the most favorable regions of the Ramachandran plot. AvBD2-K31A displays the typical three-stranded anti-parallel β-sheet of β-defensins (6-10; 18-22; 27-31) stabilized by the conserved array of 3 disulfide bridges C1-C5, C2-C4, C3-C6. An additional short anti-parallel β-strand was observed in the N-terminal part (Fig. 3). Finally, the C-terminal extremity systematically formed a final 3_{10} helix turn at the end of the molecule, whereas this turn was observed on only two of the ten AvBD2 solution structures. The assignment of all proton resonances has been deposited in the BioMagResBank (entry code 17798). Ten conformers representative of the AvBD2-K31A variant in solution have been deposited in the Protein Data Bank (2gl6 entry code).

The effects of this point mutation on the antimicrobial activity were measured. By comparison with the wild type AvBD2, the AvBD2-K31A variant exhibited a dramatic decrease in antimicrobial activity against the six bacterial strains tested, as shown by a significant increase of the MICs (Table 1). This result demonstrates the essential role played by this lysine residue at position 31 in antimicrobial activity. Furthermore, when comparing the effect of AvBD2-K31A on the Gram-positive and Gram-negative bacteria, the folded AvBD2-K31A variant was globally more damaging than the linear AvBD2 for the Gram-positive bacteria, while the opposite was observed for the Gram-negative ones. The linear form of the variant AvBD2-K31A was almost completely inactive in our conditions against all the bacterial strains (Table 1).

DISCUSSION

The aim of this work was to gain initial insights into the structure-activity relationships of avian β-defensins. We thus focused on the following three crucial questions: 1) Does AvBD2 require a chiral partner for its antimicrobial activity? 2) Is the three-dimensional structure of AvBD2 essential for the antimicrobial activity? 3) Can specific residues or features be pointed out as playing a role in the antimicrobial activity? In order to address these questions, chicken native AvBD2 and various peptides derived from its sequence were successfully synthesized in their linear or fully oxidized forms.

Involvement of a chiral partner in AvBD2 antimicrobial activity

To address the requirement of a chirality-dependent target in the antimicrobial activity, we synthesized and tested the all-D enantiomer of AvBD2. It is well established that the D-enantiomer of a native protein does not recognize the protein partners of the L-enantiomer or *vice versa* due to steric incompatibility (24,25). In the field of antimicrobial peptides, it was early shown that the all-D enantiomer homologues of magainins and cecropins exert antimicrobial potency comparable to the naturally occurring all-L peptides, which indicates the absence of a specific receptor-mediated mechanism and the achiral lipid chains of the cell membrane as the main target (26-29). By contrast, during the discovery process of the outer-membrane protein LptD as the chiral target of the peptidomimetic L27-11, it was shown that the all-D enantiomer was essentially inactive (30). The measured MICs for both D- and L-AvBD2 enantiomers are identical towards various bacterial strains, either Gram-positives or Gram-negatives (Table 1). This clearly indicates that there is no chiral requirement for the antimicrobial activity. However AvBD2 interacts with DNA in a gel shift assay (see S9 supplementary data) as reported for ostrich AvBD2 defensins (13), which share 78% of identity with chicken

AvBD2 (Fig. 1). A similar behaviour of AvBD2 and of its linear AvBD2-Acm form was observed in gel shift assays. These data suggested an unspecific interaction owing to the cationic nature of the molecules, as already noticed for most antimicrobial peptides tested *in vitro* for their binding to nucleic acids (7). Therefore the bacterial membrane appears to be the AvBD2 target.

Importance of the three-dimensional structure in AvBD2 antimicrobial activity

While the structural organization of most defensins stabilized by a network of disulfide bonds is crucial to maintain the antimicrobial activity, some linearized defensins retain their antimicrobial activity (31). On the series of bacterial strains used in our studies, the linear AvBD2-Acm peptide always proved to be less active than the fully oxidized form, indicating the requirement of the three-dimensional fold for optimal antimicrobial activity. This requirement is particularly critical for Gram-positive strains. In order to draw the first structure-activity relationships for bird defensins, we determined the three-dimensional NMR structure of chicken AvBD2. It displays the structural characteristics of β-defensins, that is a three-stranded antiparallel β-sheet, stabilized by the conserved array of three disulfide bridges (C1-C5, C2-C4, C3-C6). Most mammalian β-defensins display an additional N-terminal helix. The king penguin AvBD103b, the only avian defensin three-dimensional structure that is currently available displays a high propensity of the N-terminal part to form a helix in aqueous solution (32). By contrast, chicken AvBD2 lacks the possibility to form an N-terminal α-helix due to its shorter sequence (Fig. 1 and Fig. 2A). Hence, this helix appears to be non essential for antibacterial activity. While other studies have shown that helix conformation is essential for the action on zwitterionic lipid membranes, this structural feature appears less significant for the permeabilization of negatively charged bilayers (33-35). This helix may be involved in activity against fungi or host-cell membrane and indeed involved in selectivity, as suggested by the fungicidal activity of AvBD103b (12) compared to the lack of AvBD2 potency against *Candida albicans* (36).

Structural features

The ability of antimicrobial peptides to cross bacterial membranes and/or disrupt them is often governed by amphipathy (37-40). The analysis of the surface properties of chicken AvBD2 clearly showed that, contrary to many antibacterial molecules, AvBD2 did not display any amphipathic character (Fig. 2B and 2C), even though it contains positively charged and hydrophobic residues. This organization of positive and hydrophobic residues, which are well distributed on the three-dimensional structure of the molecule (Fig. 2), certainly provides an appropriate equilibrium to interact with bacterial membranes.

In order to determine if some of these positive and/or hydrophobic residues could play a role in this charge/hydrophobic equilibrium, the consensus sequence of the 32 avian β-defensins currently known was analyzed. As conserved residues often display a structural and/or a functional role in a given protein family, the consensus sequence was analyzed (Fig.1) in the light of chicken AvBD2 and king penguin AvBD103b three-dimensional structures (32), which share 33% of sequence identity with AvBD2. Globally, the amino acid composition of avian β-defensins is highly variable, and only the six cysteines were strictly conserved (Fig. 1). These six cysteine residues, involved in a conserved array of three disulfide bridges, ensure the high stability of the molecule and the high resistance to enzymatic degradation, and therefore undoubtedly have a structural role. For AvBD2, three half-cystines – one for each bridge - were totally embedded in the core of the protein. Their accessibility to the solvent calculated with NACCESS software (41) was 8.4, 0.0 and 0.2% for Cys8, Cys29 and Cys30, respectively. (For AvBD103b, the corresponding Cys5, Cys33 and Cys34 cysteine residues were totally embedded, with a solvent accessibility of 4.8, 0.1 and 0.3%, respectively). Subsequently, the consensus sequence highlighted two very well – but not strictly- conserved glycine residues (Gly6 and Gly21), belonging to Gly-Xaa-Cys motifs. Their role is most likely not only structural, but their presence could impact the neighboring residues: 1) Due to their small side-chain, glycines are known to be highly flexible and to have a small steric size. At position 6, the short side-chain of Gly6 prevented steric "clashes", in particular with the bulky well conserved Lys31 side chain of the "Cys-Cys-positive" motif (similarly, the totally embedded Gly10 of AvBD103b prevented steric clashes with the bulky well conserved Arg35). For two of the three exceptions not containing Gly at position 6 (Mallard Duck AvBD10 and Chicken AvBD10, see Fig. 1), the Gly-Xaa-Cys

and "Cys-Cys-positive" motifs are respectively replaced by Gly-Xaa-Xaa-Cys and "Cys-Cys-Xaa-positive" (Fig.1), which could ensure the same steric function; 2) The flexible and short side-chain of Gly21 (Gly25 for AvBD103b), conserved in all 32 avian defensins except turkey AvBD3, chicken AvBD12 and chicken Gallins, was involved in a bulge where Val20-Gly21 in the second strand of the β-sheet are facing Cys29 in the third one (Ile24-Gly25 facing Cys33 for AvBD103b). This bulge could assist in placing the neighboring Val20 residue (or Ile24 in AvBD103b) in a favorable position, and/or it could ensure the proper folding of the protein (42) and/or it could give flexibility to this part of the protein (43). It is noticeable that this bulge is present in all the mammal β-defensin three-dimensional structures presently known: human hBD1-6, bovine BD12 and mouse mBD7-8 (PDB codes 1kj5, 1fd3, 1kj6, 1zmm, 1zmp, 1zmq, 1bnb, 1e4t and 1e4r, respectively). Moreover, the consensus sequence depicted in Fig. 1 highlighted well conserved positive residues at position 4 and 31, and well conserved hydrophobic residues at position 7, 10, 18, 20 and 26 (AvBD2 numbering) which did not seem to be involved in the fold itself, and consequently could have a functional role. The role of the well conserved hydrophobic residues at position 7 (but replaced by Ser in AvBD2), or at position 10 (but replaced by Arg in AvBD103b) is tricky to extrapolate with the only two three-dimensional structures available. They probably participate in the global hydrophobic/positive properties at the surface of the protein, as do the exposed Lys4 and Phe26 (Fig. 2D). Lysine 31 was pointed out (Arg35 in AvBD103b). This positive residue keeps only its charged extremity accessible to the solvent, whereas its hydrophobic side chain is surrounded by the hydrophobic N-terminal Leu1, and the well conserved Ile18 and Val20 residues, pointing toward the solvent (Fig. 2D). A similar feature is observed for AvBD103b, where the hydrophobic part of Arg35 lies in a hydrophobic environment provided by Ile22, Ile24 and Val37 pointing toward the solvent. In the case of AvBD103b, the positively charged extremity of Arg35, accessible to the solvent, was reinforced in the three-dimensional structure by two close additional positive charges: Arg8 and Arg9.

Role of Lys31 in the antibacterial activity and the structure of AvBD2

In order to assess the structural role and to confirm - or reject - the functional role of the positively charged Lys31 in the mechanism of bacterial killing by AvBD2 and/or in its specificity towards different bacterial strains, the AvBD2-K31A variant was synthesized and studied. The point mutation of lysine 31 by an alanine residue (K31A) caused a dramatic decrease in activity (Table 1), showing the critical functional role of Lys31. However, this point mutation also causes a large structural modification in the N-terminal part of the molecule (Fig. 3), where an additional N-terminal β-stand is formed. A fine analysis of the three-dimensional models showed that the side chain interactions between the hydrophobic parts of Leu1 and Lys31, holding these residues in contact in AvBD2, are lost in the AvBD2-K31A variant. At this juncture it is not possible to precisely evaluate the contribution of these structural modifications to the decrease in activity. However, the critical functional and structural role of Lys31 has been evidenced.

Global cationicity *versus* structural distribution of charges

A common feature of most antimicrobial peptides/proteins is their net positive charge, which is essential for the initial association with bacterial membranes, through electrostatic interactions with the anionic surface of bacteria. However, the specificity of each defensin is certainly linked to its own distribution of charged and hydrophobic residues on one hand, and to the differences in the membrane composition of bacteria cell membranes on the other hand (Gram-positive *versus* Gram-negative, or between species). From our results, the global cationicity of the molecule, which is reduced in the variant form of AvBD2-K31A, appears to be more critical for Gram-negative strains. This could be explained by the higher exposure of negative charges on the Gram-negative bacterial surface due to the lipopolysaccharide. Moreover, the discrepancy we have observed in the present study between Gram-positive and Gram-negative susceptibility to linear AvBD2 might thus come from their difference in bacterial membrane accessibility and composition (44,45). However, the positive net charge of AvBD2 is one of the lowest amongst the avian β-defensins, and the AvBD2-K31A variant is charged only with three positive residues without losing all of its activity. In that variant, the loss of the three-dimensional structure has a dramatic effect on activity, as shown by the MIC of AvBD2-K31A-Acm, which was almost above the concentration range

(Table 1). Thus, even if cationicity seems to be more important in the mechanism of action of AvBD2 against the Gram-negative bacteria than against the Gram-positive ones, the role of the three-dimensional structure – and the associated distribution of positive and hydrophobic residues at the surface - predominates in the activity of this avian β-defensin. In the absence of any amphipathic character the interaction of AvBD2 with the bacterial membrane may be governed by an adequate distribution of positive and hydrophobic residues at the surface, which could be described as an appropriate partition constant (46). Recently, it has been proposed that synthetic alpha-helical amphiphilic antimicrobial peptides (47), and the amphiphilic human hBD3 (48), may act like "sand-in-a-gearbox". This mechanism of action may be based on the ability of antimicrobial peptides to disrupt over space and/or time the highly dynamics membrane-bound protein complexes involved in essential processes of bacterial life. Even if not amphiphilic, AvBD2 could show an adequate partition constant to insert into the membrane, through non-chiral non-specific interaction, and could disrupt the membrane equilibrium like sand in a gearbox.

CONCLUSION:
The similar antimicrobial activity measured for both L- and D-enantiomeric chicken AvBD2 proteins clearly indicates that there is no chiral partner for the antimicrobial activity. While the membrane emerges as the target, the resolution of the three-dimentional structure and the analysis of the AvBD2 surface revealed no amphiphilic distribution of its positively charged and hydrophobic residues. Thus, we propose that chicken AvBD2 antimicrobial activity may be based on a disorganisation of the membrane through non-chiral non-specific interaction.

Moreover, we highlighted a series of well - but not strictly - conserved residues that could be involved in the antimicrobial properties and/or in the bacterial strain specificity of bird defensins. In particular, we pointed out lysine 31 of chicken AvBD2, lying in the hydrophobic environment provided by well conserved, accessible, hydrophobic residues. The present study demonstrates the critical functional, as well as structural, role of Lys31 in antimicrobial activity.

REFERENCES

1. Selsted, M. E., and Ouellette, A. J. (2005) *Nat Immunol* **6**, 551-557
2. Yang, D., Biragyn, A., Kwak, L. W., and Oppenheim, J. J. (2002) *Trends Immunol* **23**, 291-296
3. Derache, C., Esnault, E., Bonsergent, C., Le Vern, Y., Quere, P., and Lalmanach, A. C. (2009) *Dev Comp Immunol* **33**, 959-966
4. van Dijk, A., Veldhuizen, E. J., and Haagsman, H. P. (2008) *Vet Immunol Immunopathol* **124**, 1-18
5. Powers, J. P., and Hancock, R. E. (2003) *Peptides* **24**, 1681-1691
6. Hancock, R. E., and Sahl, H. G. (2006) *Nat Biotechnol* **24**, 1551-1557
7. Marcos, J. F., and Gandia, M. (2009) *expert opin. Drug Discov.* **4**, 659-671
8. Yeung, A. T., Gellatly, S. L., and Hancock, R. E. (2011) *Cell Mol Life Sci* **68**, 2161-2176
9. European Food Safety Authority (2007) *EFSA J* **98**
10. Sadeyen, J. R., Trotereau, J., Protais, J., Beaumont, C., Sellier, N., Salvat, G., Velge, P., and Lalmanach, A. C. (2006) *Microbes Infect* **8**, 1308-1314
11. Derache, C., Labas, V., Aucagne, V., Meudal, H., Landon, C., Delmas, A. F., Magallon, T., and Lalmanach, A.-C. (2009) *Antimicrob. Agents Chemother.* **53**, 4647-4655
12. Thouzeau, C., Le Maho, Y., Froget, G., Sabatier, L., Le Bohec, C., Hoffmann, J. A., and Bulet, P. (2003) *J Biol Chem* **278**, 51053-51058
13. Sugiarto, H., and Yu, P. L. (2007) *FEMS Microbiol Lett* **270**, 195-200
14. Cadene, M., and Chait, B. T. (2000) *Anal Chem* **72**, 5655-5658
15. Gabant, G., and Cadene, M. (2008) *Methods* **46**, 54-61

16. Lehrer, R. I., Rosenman, M., Harwig, S. S., Jackson, R., and Eisenhauer, P. (1991) *J Immunol Methods* **137**, 167-173

17. Delaglio, F., Grzesiek, S., Vuister, G. W., Zhu, G., Pfeifer, J., and Bax, A. (1995) *J Biomol NMR* **6**, 277-293.

18. Johnson, B. A., and Blevins, R. A. (1994) *J Biomol NMR* **4**, 603-614

19. Wüthrich, K. (1986) *NMR of proteins and nucleic acids.*, New York

20. Linge, J. P., O'Donoghue, S. I., and Nilges, M. (2001) *Methods Enzymol* **339**, 71-90

21. Koradi, R., Billeter, M., and Wuthrich, K. (1996) *J Mol Graph* **14**, 51-55, 29-32

22. Cremer, G. A., Tariq, H., and Delmas, A. F. (2006) *J Pept Sci* 12, 437-442

23. Boisbouvier, J., Blackledge, M., Sollier, A., and Marion, D. (2000) *J Biomol NMR* **16**, 197-208

24. Milton, R. C., Milton, S. C., and Kent, S. B. (1992) *Science* **256**, 1445-1448

25. Wei, G., de Leeuw, E., Pazgier, M., Yuan, W., Zou, G., Wang, J., Ericksen, B., Lu, W. Y., Lehrer, R. I., and Lu, W. (2009) *J Biol Chem* **284**, 29180-29192

26. Wade, D., Boman, A., Wahlin, B., Drain, C. M., Andreu, D., Boman, H. G., and Merrifield, R. B. (1990) *Proc Natl Acad Sci U S A* **87**, 4761-4765

27. Casteels, P., and Tempst, P. (1994) *Biochem Biophys Res Commun* **199**, 339-345

28. Castle, M., Nazarian, A., Yi, S. S., and Tempst, P. (1999) *J Biol Chem* **274**, 32555-32564

29. Chen, J., Falla, T. J., Liu, H., Hurst, M. A., Fujii, C. A., Mosca, D. A., Embree, J. R., Loury, D. J., Radel, P. A., Cheng Chang, C., Gu, L., and Fiddes, J. C. (2000) *Biopolymers* **55**, 88-98

30. Srinivas, N., Jetter, P., Ueberbacher, B. J., Werneburg, M., Zerbe, K., Steinmann, J., Van der Meijden, B., Bernardini, F., Lederer, A., Dias, R. L., Misson, P. E., Henze, H., Zumbrunn, J., Gombert, F. O., Obrecht, D., Hunziker, P., Schauer, S., Ziegler, U., Kach, A., Eberl, L., Riedel, K., DeMarco, S. J., and Robinson, J. A. (2010) *Science* **327**, 1010-1013

31. Hoover, D. M., Wu, Z., Tucker, K., Lu, W., and Lubkowski, J. (2003) *Antimicrob Agents Chemother* **47**, 2804-2809

32. Landon, C., Barbault, F., Legrain, M., Menin, L., Guenneugues, M., Schott, V., Vovelle, F., and Dimarcq, J. L. (2004) *Protein Sci* **13**, 703-713

33. Dathe, M., and Wieprecht, T. (1999) *Biochim Biophys Acta* **1462**, 71-87

34. Epand, R. F., Lehrer, R. I., Waring, A., Wang, W., Maget-Dana, R., Lelievre, D., and Epand, R. M. (2003) *Biopolymers* **71**, 2-16

35. Papo, N., and Shai, Y. (2003) *Peptides* **24**, 1693-1703

36. Harwig, S. S., Swiderek, K. M., Kokryakov, V. N., Tan, L., Lee, T. D., Panyutich, E. A., Aleshina, G. M., Shamova, O. V., and Lehrer, R. I. (1994) *FEBS Lett* **342**, 281-285

37. Papo, N., and Shai, Y. (2005) *J Biol Chem* **280**, 10378-10387

38. Rosenfeld, Y., Sahl, H. G., and Shai, Y. (2008) *Biochemistry* **47**, 6468-6478

39. Yount, N. Y., Bayer, A. S., Xiong, Y. Q., and Yeaman, M. R. (2006) *Biopolymers* **84**, 435-458

40. Brogden, K. A. (2005) *Nat Rev Microbiol* **3**, 238-250

41. Hubbard, S. J., and Thornton, J. M. (1993) NACCESS. *(*of, D., and Biochemistry and Molecular Biology, U. C. L. eds.)

42. Xie, C., Prahl, A., Ericksen, B., Wu, Z., Zeng, P., Li, X., Lu, W. Y., Lubkowski, J., and Lu, W. (2005) *J Biol Chem* **280**, 32921-32929

43. Paquet, F., Loth, K., Meudal, H., Culard, F., Genest, D., and Lancelot, G. (2010) *FEBS J* **277**, 5133-5145

44. Nikaido, H. (1994) *Science* **264**, 382-388

45. Raetz, C. (1987) Structure and biosynthesis of lipid A in E.coli. in *Escherichia coli and Salmonella typhimurium: Cellular and Molecular Biology (*Neidhart, F. C. ed., ASM Press, Washington D.C.

46. Melo, M. N., Ferre, R., and Castanho, M. A. (2009) *Nat Rev Microbiol* **7**, 245-250

47. Pag, U., Oedenkoven, M., Sass, V., Shai, Y., Shamova, O., Antcheva, N., Tossi, A., and Sahl, H. G. (2008) *J Antimicrob Chemother* **61**, 341-352

48. Sass, V., Pag, U., Tossi, A., Bierbaum, G., and Sahl, H. G. (2008) *Int J Med Microbiol* **298**, 619-633

FOOTNOTES

FIGURE LEGENDS

Fig. 1: Alignment of the 32 avian defensin sequences currently referenced in Uniprot. Dots were inserted for alignment purpose. Left: protein name; right: Uniprot entry name and accession number; Top: Consensus sequence. Conserved residues are indicated in the consensus sequence, "h" standing for conserved hydrophobic residues, "+" standing for conserved positive residues.

Fig. 2: Chicken AvBD2 Global fold and surface potentials. **A:** Superimposition of the 10 models representative of chicken AvBD2 solution structure with the three-stranded antiparallel β-sheet drawn in blue (drawn with MOLMOL software (21); **B:** Hydrophobic and hydrophilic potential areas, calculated with the MOLCAD option of SYBYL software (TRIPOS Inc., St. Louis, MO) at the Connolly surfaces, are displayed in brown and blue, respectively. Green surfaces represent an intermediate hydrophobicity (scale -0.18, +0.18); **C:** Electrostatic positive and negative areas, calculated with the SYBYL software at the Connolly surfaces, are displayed in red and blue, respectively. Intermediate areas are in green (scale -230, +230 kcal.mol-1); **D:** Schematic representation of one structure: disulfide bridges in yellow; hydrophobic (Phe10, Ile18, Val20, Phe26) and positive (Lys4, Lys31) well conserved residues in blue and red, respectively. The last 2 residues of the consensus sequence (Gly6 and Gly21) were omitted for clarity.

Fig. 3: Left: Schematic representation of chicken AvBD2-K31A variant backbone and disulfide bridges. The three typical strands of β-defensin (in grey) are numbered β1 to β3. The additional N-terminal β-strand and the C-terminal turn are drawn in black; Right : Superimposition of AvBD2 (light grey) and AvBD2-K31A (dark grey) structures (drawn with MOLMOL Software)

Table 1: Antibacterial activity of AvBD2 peptides. The minimal inhibitory concentration (MIC) was determined by radial diffusion assay for every bacterial strain. The statistical difference between L-AvBD2 and each peptide MIC was assessed by comparing the slope and intercepts of both regression lines with GraphPad Prism 5 software (GraphPad Software).

Table 2: Structural statistics for the ten final models of chicken AvBD2, and AvBD2-K31A variant.

Fig. 1


```
                              cons                    c+...GhC.h.C......h.hG.C...h..CC+       Entry name|Accession

Chicken AvBD2                                                                                GLL2_CHICK|P46158
Ostrich AvBD2                 LFCKG..GSCHFGGCP..SHLIKVGSCF.GFRSCCKWPWNA                      OSTR1_STRCA|P85113
Turkey AvBD2                  LFCRK..GTCHFGGCP..AHLVKVGSCF.GFRACCKWPWDV                      AMP2_MELGA|P80392
Mallard duck AvBD2  MRILYLLFSLLFLALQVSPGLSSPKRDMLFCKR..GTCHFGRCP..SHLIKVGSCF.GFRSCCKWPWDA   Q4VSK2_ANAPL|Q4VSK2
Mallard duck AvBD2  MRILYLLFSVLFLVLQVSPGLSLPQRDMFLCRI..GSCHFGRCP..IHLVRVGSCF.GFRSCCKSPWDV   B7UB88_ANAPL|B7UB88
                    MRILYLLFSVLFLVLQVSPGLSLPQRDMFLCRK..GSCHFGRCP..IHLIKVGSCF.GFRSCCKSPWDV

King penguin AvBD103b                                                                        SPHE2_APTPA|P83430
King penguin AvBD103a         SFGLCRLRRGFCARGRCR..FPSIPIGRCS.RFVQCCRRVW                      SPHE1_APTPA|P83429
Chicken AvBD3                 SFGLCRLRRGFCAHGRCR..FPSIPIGRCS.RFVQCCRRVW                      GLL3_CHICK|Q9DG58
Turkey AvBD3   MRIVYILLIPFFLLFLQGAAGTATQCRIRGGFCV:GSCR..FPHIAIGKCA.TFISCGRAYEVDALNSVRTSPWLLAPGNNPH  Q9DG57_MELGA|Q9DG57
Turkey AvBD1         MRIVYILLFPFFLLFLQSAAGTPIQCRIRGGFCRFGSCR..FPHIAIAKCA.TFIPCCGSIWG          AMP1_MELGA|P80391
Chicken AvBD1  MRIVYILLFPFILLLAQGAAGSSLALGKREKCLRRNGFCAFLKCP..TLSVISGTCS.RFQVCCKTLLG           AMP1_CHICK|P80389
Chicken AvBD1                 GRKSDCFRKSGFCAFLKCP..SLTLISGKCS.RFYLCCKRIR                     GLL1_CHICK|P46156
Chicken AvBD1a                GRKSDCFRKSGFCAFLKCP..SLTLISGKCS.RFYLCCKRIWG                    GLL1A_CHICK|P46157
Ostrich AvBD1  MRIVYILLPFILLLAQGAAGSSQALGRKSDCFRKNGFCAFLKCP..YLTLISGKCS.RFHLCCKRIWG            OSTR2_STRCA|P85114
Chicken AvBD5                 APGNKAECEREKGYCGFLKCS..FPFFVSGKCS.RFFFCCKNIW                   GLL5_CHICK|Q6IV26
Chicken AvBD4   MQILTLLFAVILLMLRAEPGLSLARGLPQDCERRGGFCSHKSCP..PGIGRIGLCS.KEDFCCRSRWYS          GLL4_CHICK|Q6GXJ1
Ostrich AvBD7  MKILCFFIVLLFVAVHGAVGFSRSPRYHMQCGYRGTFCTPGKCP..HGNAIGLCR.PKYSCCRWL              OSTR3_STRCA|P85115
Ostrich AvBD8                 LPRPLDPCIAQNGRCFTGICR..YPYFWIGTCR.NGKSCCRRR                    OSTR4_STRCA|P85116
                              LPVNEAQCRQVGGYCGLRICN..FPSRFLGLCT.RNHPCCSRVWV

Chicken AvBD7                 QPFIPRPIDTCRLRNGICFPGICR..RPYIWIGTCNNGIGSCCARGWRS              GLL7_CHICK|Q6QLR2
Chicken AvBD6   MRILYLLLSVLFVVLQGVAGQPYFSSPIHACRYQRGVCIFGPCR..WPYYRVGSCGSGLKSCCVRNRWA          GLL6_CHICK|Q6QLR3
Mallard duck AvBD9  MRILFFLVAVLFFLFQAAPAYSQEDADTLACRQSHGSCSFVACR..APSVIGTCRGGKLKCCKWAPSS       A3FPG7_ANAPL|A3FPG7
Chicken AvBD9   MRILFFLVAVLFFLFQAAPAYSQEDADTLACRQSHGSCSFVACR..APSVIGTCRGGKLKCCKWAPSS          GLL9_CHICK|Q6QLR1
Quail AvBD9     MRILFFLVAVLFFLFQAAPAYSQEDPDTLACRQHGSCSFVACR..APSVIGTCRGGKLKCCKWAPSS          D0F1S0_COTCO|D0F1S0
Mallard Duck AvBD10            VLLFLFQAAPGSADAPFADTAACRSGNFCRAGACP..PTFRASGSCHGGLLNCCAK        B5AAX3_ANAPL|B5AAX3
Chicken AvBD10  MKRILCLLFAVLLFLFQAAPGSADFLFPDTVACRTCGNFCRAGACP..PTFTISGQCHGGLLNCCAKIPAQ        GLL10_CHICK|Q6QLQ9
Chicken AvBD14     MGIFLLFIVLLAVPQAAPESDTVTCRKMKGKCSFLLCP..FFKRSSGTCYNGLAKCCRPFW               GLL14_CHICK|Q0E4V3
Chicken AvBD12     MRNLCFVFIFISLLAHGSTHGPDSCNHDRGLCRVNCN..PGEYLAKYCFBFVILCCKPLSPTPTKT          GLL12_CHICK|Q6QLQ7

Chicken Gallin  MRFLCLVFAVLLVSLAAPGYGLVLKYCPK.IGYCS.NTCSKTQIWATSHGCK.MY..CLPASWKWK             D5GR58_CHICK|D5GR58
Chicken Gallin  MRFLCLVFTVLLLVSLAAPGYGLVLKYCPK.IGYCS.NTCSKTQIWATSHGCK.MY..CLPASWKWK            D5GR60_CHICK|D5GR60
Chicken AvBD8  MKILYLLLAVLITVLQSSLGFMRVPNNEACQEQAGGICSKDHCF.HLHTRAFGHCQ.RGVFCCRTVYD            GLL8_CHICK|Q6IV23
Chicken AvBD13  MRILQLLFAIVVILLLQDAPARGFSDSQLCRNHGHCR.RLCF.HMESWAGSCMNGRLRCCRFSTKQPFSNPKHSVLHTAEQDPSPSLGGT  GLL13_CHICK|Q6IV18

Chicken AvBD11  MKLFSCLMALLLFLLQAVPGLGLPRDTSRCVGYHGYCIRSKVCP.KPFAAFGTCSWRQKTCCVDTTSDFHTCQDKGGHCGHVSPKIRCLEEQLGICPLKRWTCCKEI  GLL11_CHICK|Q6IV20
```

14

Fig. 2

Fig. 3

Table1

<div align="center">

MIC in μM
95% confidence interval

</div>
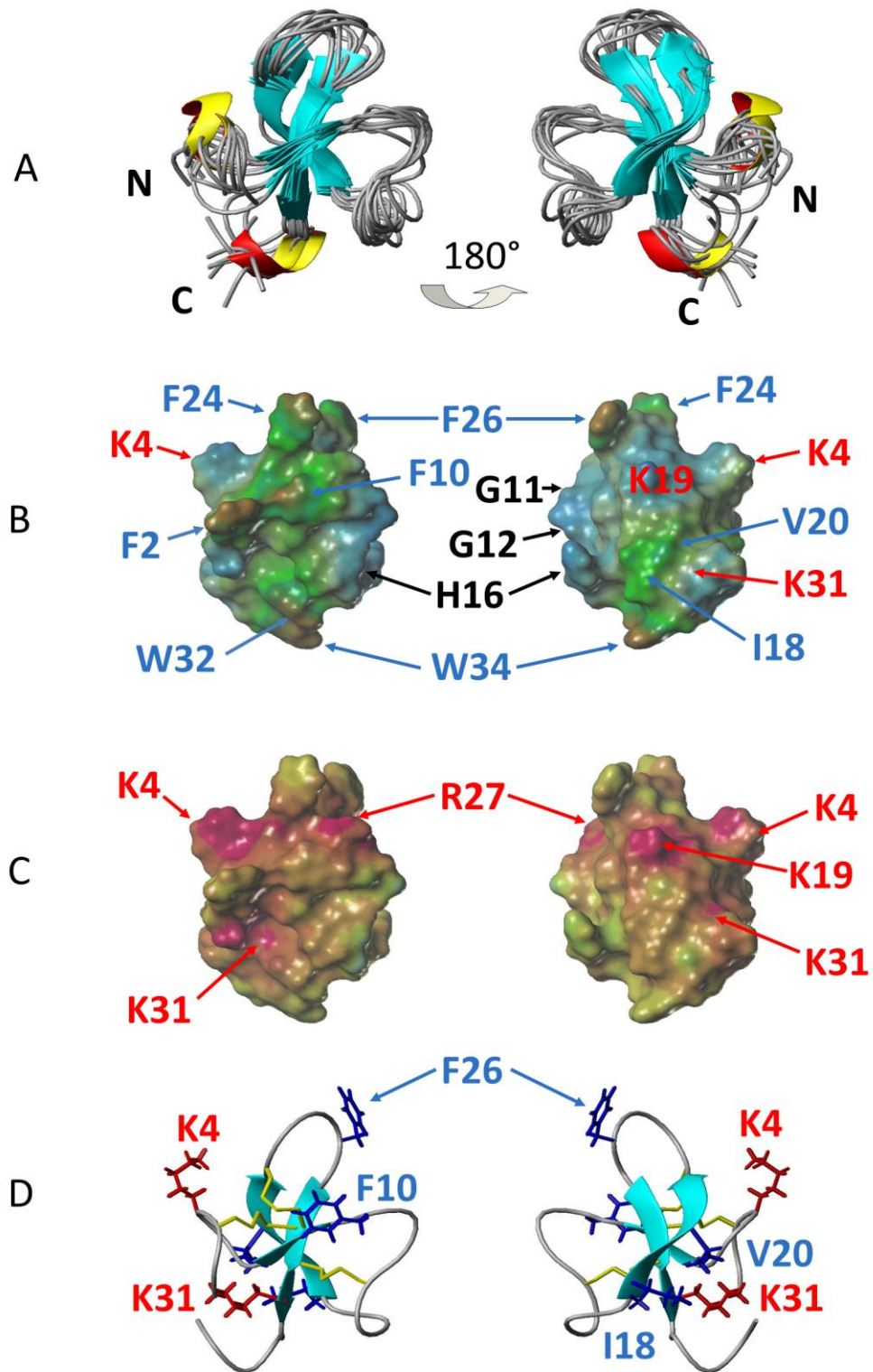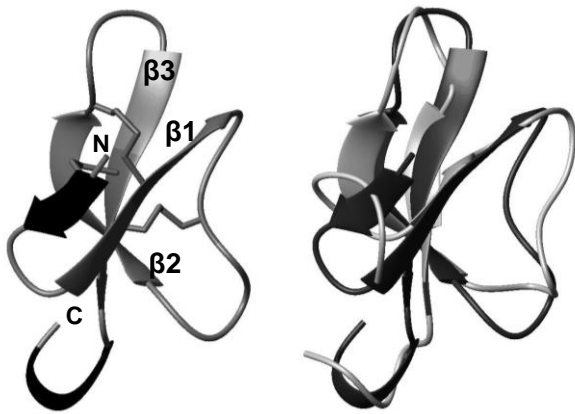
Bacterial strains	L-AvBD2	D-AvBD2	L-AvBD2-Acm	AvBD2-K31A	AvBD2-K31A-Acm
Gram +					
B. cereus	**0.31**	**0.34**	**3.47**[a]	**0.75**[b]	**>58.26**
	0.19-0.47	0.19-0.53	2.12-4.87	0.56-0.97	
L. monocytogenes	**0.20**	**0.20**	**3.21**[a]	**1.55**[c]	**23.3-58.26**
	0.09-0.36	0.11-0.34	0.98-6.13	1.05-2.14	
S. aureus	**0.58**	**1.37**	**>114.99**	**6.56**[c]	**>116.52**
	0.05-1.79	0.35-3.03		0-32.5	
Gram -					
E. coli	**1.09**	**1.05**	**1.23**	**2.07**[d]	**23.3-58.26**
	0.68-1.57	0.73-1.40	0.32-2.49	0.11-5.20	
S. Enteritidis	**0.48**	**0.52**	**1.31**[c]	**2.55**[c]	**>58.26**
	0.20-0.86	0.26-0.87	0.64-2.13	0.77-4.64	
S. Typhimurium	**3.67**	**1.59**	**5.18**[a]	**7.08**[c]	**>58.26**
	1.73-5.99	1.83-5.96	0-6.06	0.57-10.23	

[a] , P=0.0002, [b] , P=0.0003, [c] , P<0.0001, [d] , P=0.016.

Table 2

	AvBD2	AvBD2-K31A
Noe restraints		
Total	530	1069.1
Intraresidue ($|i\text{-}j| = 0$)	278.7	295.7
Sequential ($|i\text{-}j| = 1$)	112.3	261.1
Medium range ($2 \leq |i\text{-}j| \leq 4$)	29.2	170.5
Long range ($|i\text{-}j| \geq 5$)	109.8	341.8
Disulfide bridges	Introduced as constraints	Ambiguous disulfide bridges option
RMSD on backbone Cα atoms (pairwise, Å)		
Global (2-35)	1.88 ± 0.48	0.37 ± 0.11
Triple-stranded β-sheet	0.62 ± 0.13	0.19 ± 0.04
β1	0.32 ± 0.20	0.14 ± 0.05
β2	0.35 ± 0.12	0.11 ± 0.03
β3	0.28 ± 0.11	0.09 ± 0.03
Ramachandran plot[1] (%)		
Most favored & additional allowed regions	92.7	96.2
Generously allowed regions	6.2	3.8
Disallowed regions	1.1	0
Energies[2] (kcal.mol-1)		
Electrostatic	-1103 ± 90	-1033 ± 66
van der Waals	-102 ± 19	-76 ± 6
ENOE	11 ± 5	36 ± 4
Total energy	-1024 ± 100	-738 ± 46

[1] Determined by PROCHECK
[2] Calculated with the standard parameters of ARIA

Figure S1: Folding kinetics of ʟ-AvBD2 monitored by HPLC with a linear gradient (25-40%, 1ml/min) of MeCN in 0.1% TFA over 30 min. Absorbance at 214 nm. R: reduced; O: oxidized
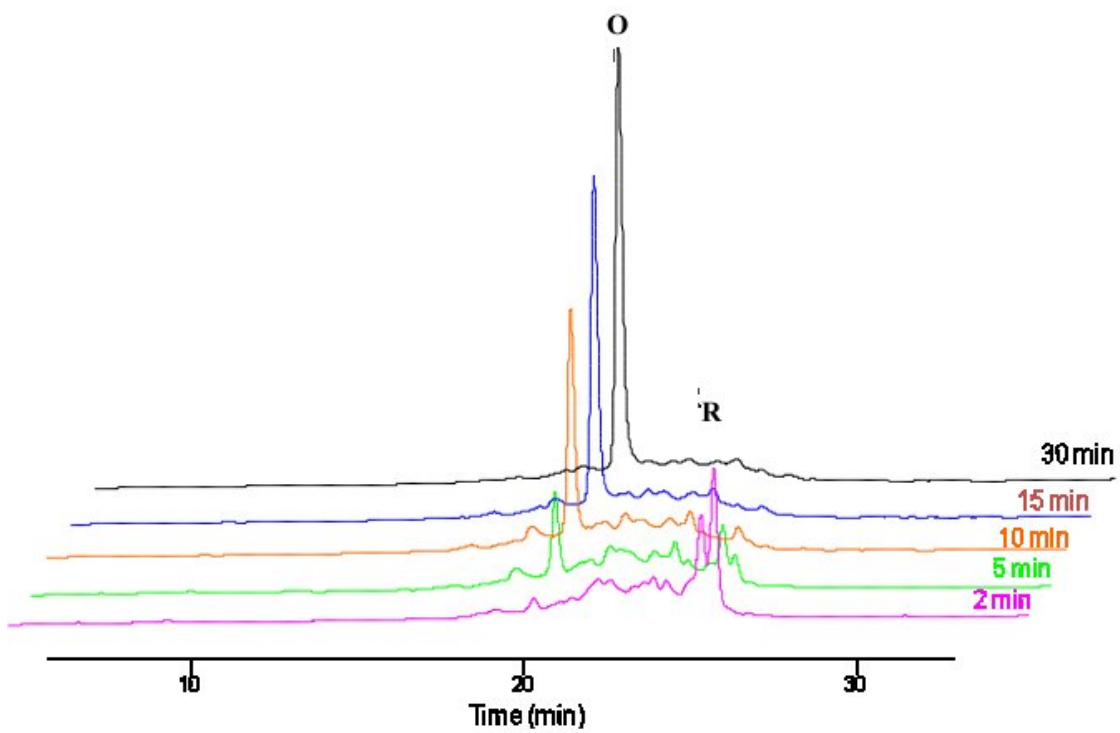
Figure S2: Co-injection of the natural and synthetic AvBD2 peptides in RP-HPLC. Gradient : 25-40% B over 30 min ; Absorbance at 214 nm. Natural AvBD2 was obtained from the chicken bone marrow (11).
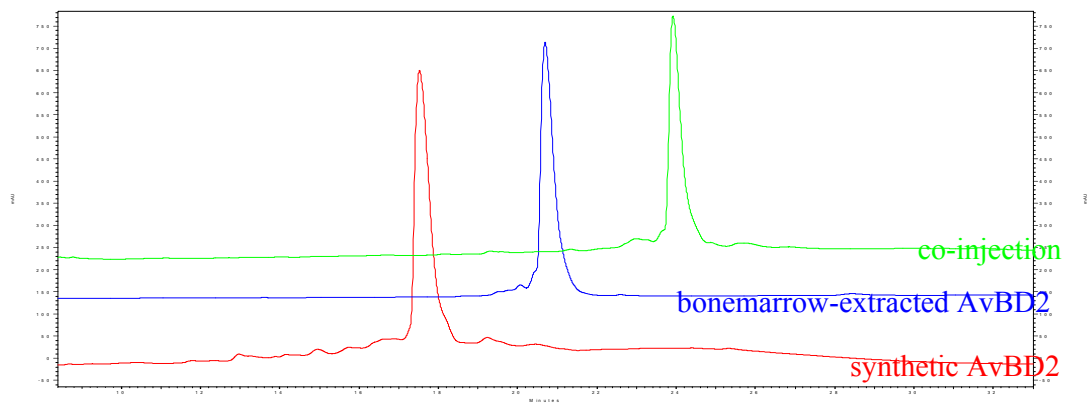
Table S1: Antimicrobial activity of natural AvBD2 and synthetic AvBD2

| Bacterial strains	Radial diffusion assay MIC in μM 95% confidence interval	
	Natural AvBD2	Synthetic AvBD2
Gram+		
B. subtilis	**0.28** 0.19-0.39	**0.31** 0.17-0.51
B. cereus	**0.47** 0.29-0.70	**0.51** 0.25-087
S. aureus	**0.42** 0.14-0.86	**0.53** 0.06-1.41
S. haemolyticus	**0.25** 0.12-0.43	**0.38** 0.26-0.53
S. saprophyticus	**0.22** 0.09-0.42	**0.24** 0.09-0.46
L. monocytogenes	**0.22** 0.08-0.43	**0.20** 0.09-0.37
Gram-		
S. Enteritidis ATCC14026	**0.80** 0.47-1.22	**0.60** 0.25-1.08
S. Enteritidis LA5	**6.05** 3.45-8.88	**5.33** 2.24-8.92
S. Typhimurium	**2.39** 0.75-4.66	**3.07** 1.28-5.33
E. cloacae	**> 64**	**> 64**
K. pneumoniae	**0.71** 0.26-1.40	**0.83** 0.35-1.53
E. coli	**0.72** 0.50-1.00	**0.68** 0.50-0.89
P. aeruginosa	**1.86** 0.75-3.36	**2.18** 0.97-3.74

Figure S3: Characterization of the AvBD2 peptides by HPLC and MALDI-TOF MS. Elution on a C18 reversed phase column (300 Å) with a linear gradient (solvent A: H_2O containing 0.1% TFA; solvent B: MeCN containing 0.1% TFA) at a flow rate of 1 mL/min. MALDI/TOF: matrix used; α-cyano-4-hydroxy-cinnamic acid (HCCA), co-crystallized using the dry droplet method.
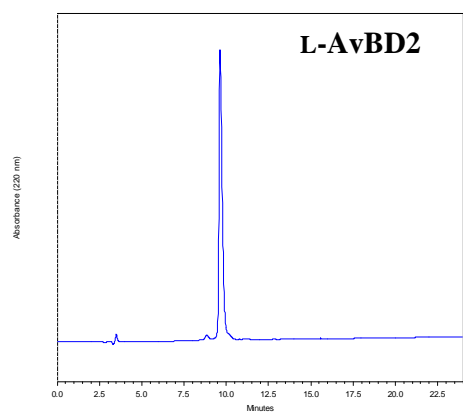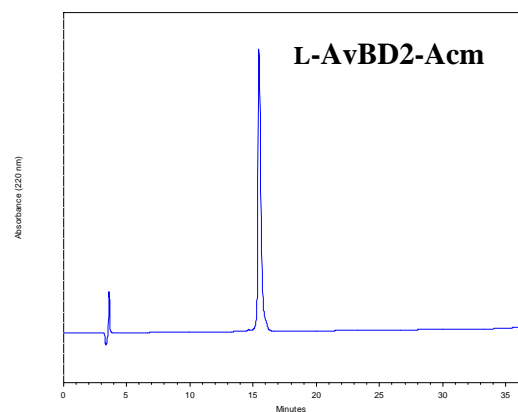

Gradient: 30-45% B over 20 min
m/z: 3912.67 calculated for
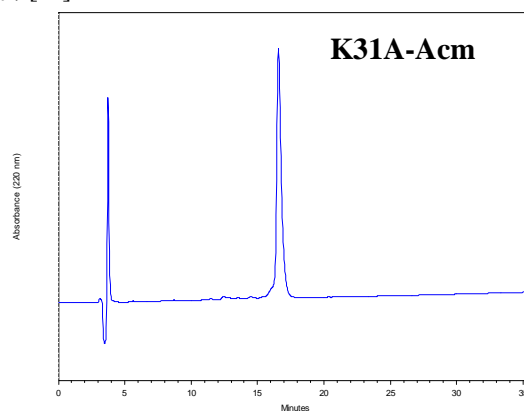$C_{176}H_{249}N_{49}O_{42}S_6$; [M]: 3911.72
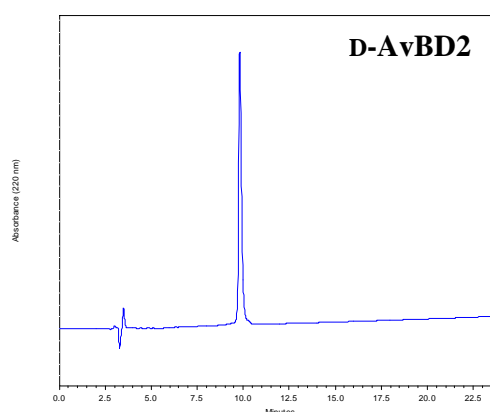
30-45% B over 20 min
m/z: 3912.68 calculated for
$C_{176}H_{249}N_{49}O_{42}S_6$; [M]: 3911.72
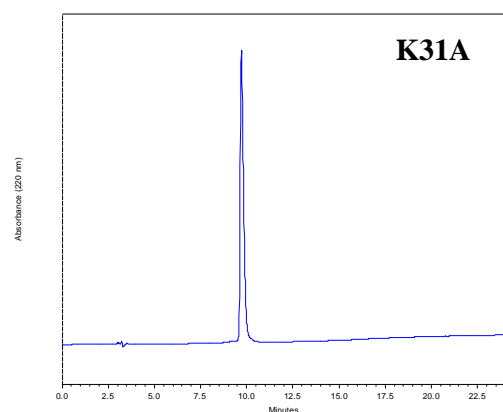
Gradient: 30-45%B over 20 min
m/z:3855.70 calculated for
$C_{173}H_{242}N_{48}O_{42}S_6$; [M]: 3854.66

Gradient: 25-50%B over 30 min
m/z:4346.1 calculated for $C_{194}H_{285}N_{55}O_{48}S_6$; [M]: 4344.99

Gradient: 25-50%B over 30 min
m/z:4288.56 calculated for
$C_{191}H_{278}N_{54}O_{48}S_6$; [M]: 4287.99

4

Figure S4: Comparison of the CD spectra obtained for L-AvBD2 (blue), D-AvBD2 (red).
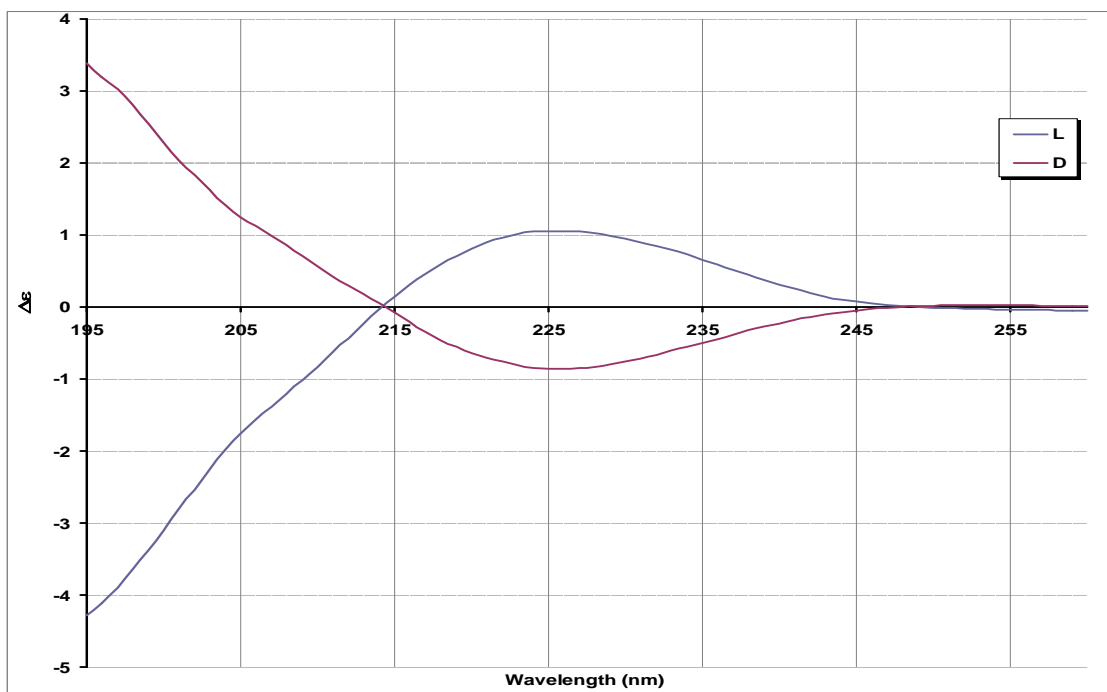
Table S2: Influence of different co-solvents on the folding yield of AvBD2 peptides. The oxidative foldings (50 µg/ml peptide concentration) were performed at a peptide/GSH/GSSG molar ratio of 1/100/10 in deoxygenated 100 mM Tris-HCl buffer pH 8.5 containing 1 mM EDTA, in 50% iPrOH, MeOH or MeCN, or without co-solvent. The conversion yields were determined by integrating the HPLC peaks (λ=280nm) corresponding to linear AvBD2 (t = 0) and folded AvBD2 (t= 60 min), keeping constant the injection volumes. The linear/folded ratio is expressed as a percentage.

Peptides	Co-solvent			
	none	iPrOH	MeOH	MeCN
L-AvBD2 and D-AvBD2	59	74	74	74
AvBD2-K31A	8	47	39	42

Table S3: Determination of disulfide-connected peptides using PeptideMap. The tolerance over statistical error on mass/charge values was set at 45 ppm.

Proteinase	Observed mass/charge	Interpretation	Links - Free SH	Theoretical mass/charge for charge equal to 1	Measure- ment error
Papain	1641.807	$[G_5\text{-}G_{12}]$ — $[L_{17}\text{-}G_{25}]$	1 - 0	1641.816	-0.009
Trypsin	947.369	$[L_1\text{-}K_4]$ — $[S_{28}\text{-}K_{31}]$	1 - 1	947.396	-0.019
	2369.036	$[G_5\text{-}K_{19}]$ — $[V_{20}\text{-}R_{27}]$	1 - 1	2369.074	-0.038
	2444.015	$[L_1\text{-}K_4]$, $[G_5\text{-}K_{19}]$ and $[S_{28}\text{-}K_{31}]$	2 - 1	2444.080	-0.065
	2806.219	$[G_5\text{-}K_{19}]$, $[V_{20}\text{-}R_{27}]$, and $[S_{28}\text{-}K_{31}]$	2 - 1	2806.214	0.005

Figure S5: Disulfide bridges as deduced from mass spectrometry data (see Table S6). Links in blue are deduced from possibilities remaining after deductions from individual proteolysis experiments.
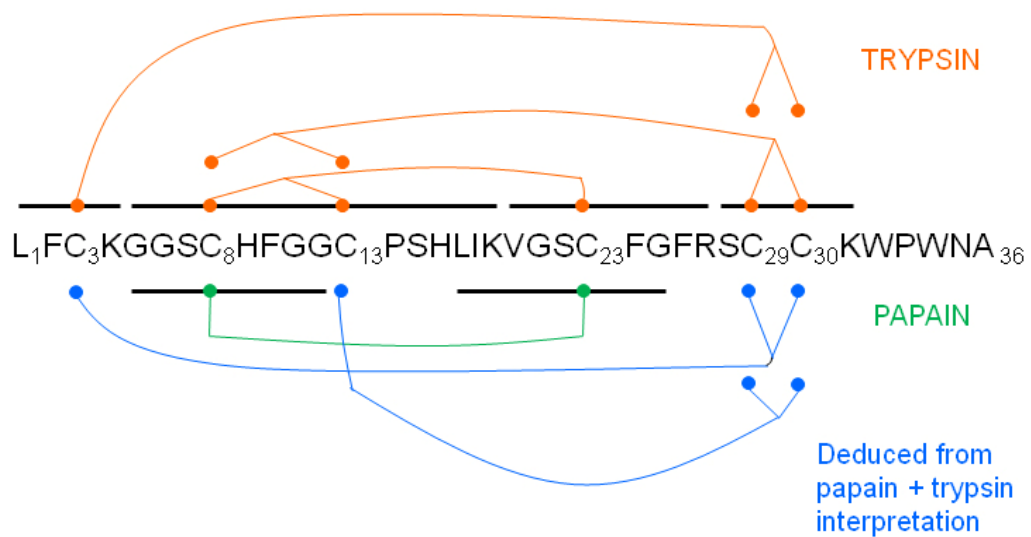
Figure S6: Interactions between DNA (100ng/lane) and AvBD2 peptides. Lane 1, DNA:Peptide ratio1 : 0; lane 2, DNA:Peptide ratio 1 : 0.5; lane 3,DNA:peptide ratio 1 : 1; lane 4, DNA:peptide ratio 1 : 2; lane 5, DNA:peptide ratio 1 : 4 ;lane 6, DNA:peptide ratio 1 : 6; lane 7, DNA:peptide ratio 1 : 8; lane 8, DNA:peptide ratio 1 : 0.1; lane 9, DNA:peptide ratio 1 : 0.5; lane 10, DNA:peptide ratio 1 : 1; lane 11, DNA:peptide ratio 1 : 1.5. DNA used for this test was the plasmid pET14b (4671 pb, Novagen). The plasmid was mixed with 10 X buffer comprising of 100 mM Tris pH 8, 200 mM KCl, 10 mM EDTA, glycerol, water and peptides at increasing concentrations. The archaeal MC1 protein (De Vuyst, G., Aci, S., Genest, D., and Culard, F., Atypical recognition of particular DNA sequences by the archaeal chromosomal MC1 protein. *Biochemistry* **44** (30), 10369 (2005) was used for comparison because this peptide had previously been shown to bind to DNA fragments. The solutions were incubated at room temperature for an hour. To separate the DNA fragments, the samples were loaded onto a 1% agarose/TBE (89 mM Tris Base, 89 mM Boric acid, 2 mM EDTA) gel and run at 100 V for 55 min. The gel was then stained with 1µg/mL ethidium bromide in TBE.